Electrical conductance of silver nanoparticles grown in glass-ceramic

1990 J. Phys.: Condens. Matter 2 9323

(http://iopscience.iop.org/0953-8984/2/47/007)

J. Phys.: Condens. Matter **2** (1990) 9323–9334. Printed in the UK

Electrical conductance of silver nanoparticles grown in glass–ceramic

B Roy and D Chakravorty
Indian Association for the Cultivation of Science, Jadavpur, Calcutta 700032, India

Received 1 March 1990, in final form 20 June 1990

Abstract. Conducting films consisting of silver particles of diameters ranging from 4 to 12 nm have been grown in glass–ceramic by subjecting the latter to a $Li^+ \rightleftharpoons Ag^+$ exchange followed by a suitable reduction treatment. The DC electrical resistance of these films has been measured over the temperature range 80–300 K. The resistivity data have been analysed in terms of the Ziman theory of electron–phonon scattering. The effective Debye temperature Θ_p has been estimated by fitting the experimental data to Ziman's equation. Θ_p is seen to vary from 98 to 192 K for silver particle sizes ranging from 4.3 to 11.0 nm. The silver particle aggregates in the present system have a fractal microstructure with fractal dimensions of around 1.6 and 1.9, respectively.

1. Introduction

The physics of particles having nanometre dimensions has attracted considerable attention in recent years (Marlow 1982). Such ultrafine particles are expected to exhibit novel properties not found in the bulk material (Novotny and Meincke 1973). Several attempts have been made to find a large value of static polarizability in an assembly of ultrafine metal particles (Meier and Wyder 1972, Dupree and Smithard 1972, Strassler and Rice 1972) which was predicted earlier on theoretical grounds by Gorkov and Eliashberg (1965). An enormous yield of photoelectrons from silver nanoparticles has been demonstrated (Schmitt-Ott *et al* 1980). Luminescence spectra of glasses containing nanoparticles of CdS and CdSe reveal large electronic energy shifts relative to bulk energy levels due to the quantum confinement effect (Warnock and Awschalom 1985). Large non-linear optical polarizability is shown by nanocomposites consisting of semiconductor microcrystallites embedded in a borosilicate glass (Hanamura 1988). Optical absorption of nanometre-sized metal particles dispersed in an insulating medium has been studied extensively because of its applications concerning photothermal conversion devices (Anderson *et al* 1980). The effect of particle size on the electrical resistivity of ultrafine metal grains has been investigated (Fujita *et al* 1969, 1976). These studies have been carried out on silver and aluminium thin films, respectively, the particle size being of the order of 10 nm or more. The results show a phonon softening effect due to the small size of the metal particles.

An ion-exchange technique was developed earlier in our laboratory to induce an electrically conducting silver film on suitably chosen glass–ceramic samples (Das *et al* 1978; Chakravorty and Roy 1985). In this method the glass–crystal interface is believed

0953-8984/90/479323 + 12 $03.50

to act as the nucleation sites for the growth of silver particles during the reduction stage. This effect has also been observed in photosensitive glasses in which the crystalline phase is developed by selective ultraviolet irradiation followed by a suitable heat treatment (Trotter and Smith 1984). We have now used the ion-exchange method to grow, within a glass–ceramic, electrically conducting films consisting of silver particles of diameters ranging from 4 to 12 nm. The electrical resistance of these films have been measured and analysed in terms of existing theories. The results are reported in this paper.

2. Experimental details

The composition of the glass used in this study was 55 mol% SiO_2–12 mol% ZnO–32.2 mol% Li_2O–0.8 mol% P_2O_5; P_2O_5 is a nucleating agent which enhances the rate of crystallization of the different phases within the glass matrix. The glass was prepared from reagent-grade chemicals. A mixture of the required amounts of various chemicals was melted in alumina crucibles in an electrically heated furnace at around 1400 °C. Glass plates of approximate dimensions 3 cm × 2 cm × 1 cm were cast by pouring the melt onto a brass plate.

For ceramization of the glass sample it is subjected to heat treatment at the nucleation and growth temperatures, respectively, as determined by differential thermal analysis (DTA) and reported earlier (Chakravorty and Roy 1985). From the latter the nucleation temperature is chosen as 565 °C. There are two crystallization (growth) temperatures: 630 and 825 °C. Two heat treatment schedules have been tried:

(i) 565 °C for 1 h followed by 630 °C for 3 h;
(ii) 565 °C for 1 h followed by 630 °C for 3 h followed by 825 °C for 3 h.

We find that both the schedules precipitate two crystalline phases without any appreciable difference in the glass–ceramic microstructure. We have therefore used the first heat treatment schedule in our sample preparation. The crystalline phases are identified from the x-ray diffraction patterns obtained with a Phillips PW 1051 diffractometer using the Cu Kα line.

For the ion-exchange step, surfaces of glass–ceramic samples of approximate dimensions 4 mm × 2 mm × 1 mm are polished using silicon carbide grit of mesh size 800 followed by 0.05 μm Al_2O_3 powder. The polished samples are subjected to a lithium $\rightleftharpoons$ silver exchange by immersing them in a molten bath of silver nitrate contained in a Pyrex boat at a temperature of 310 °C for a period of 8 h. After the interdiffusion run the samples are washed in distilled water to remove any silver nitrate adhering to their surfaces. The ion-exchanged samples are then reduced in hydrogen at temperatures varying from 320 to 600 °C for a duration ranging from 5 min to 1 h. The specimens after the reduction run are quenched to room temperature to ensure a narrow size distribution of the silver metal particles.

Transmission electron microscopy of different specimens is carried out with a JEM 200 CX microscope operated at 100 kV. The details of sample preparation are to be found elsewhere (Chatterjee and Chakravorty 1989).

The surface resistance of the glass–crystal–metal composite is measured by a conventional four-probe method (Fujita *et al* 1969) over the temperature range 80–300 K. Two strips of silver Electrodag 1415 (supplied by Acheson Colloiden B.V., Holland) painted on the conducting surface at a separation of about 1 mm act as the voltage terminals. Silver-painted end surfaces of the specimen act as current terminals. As the

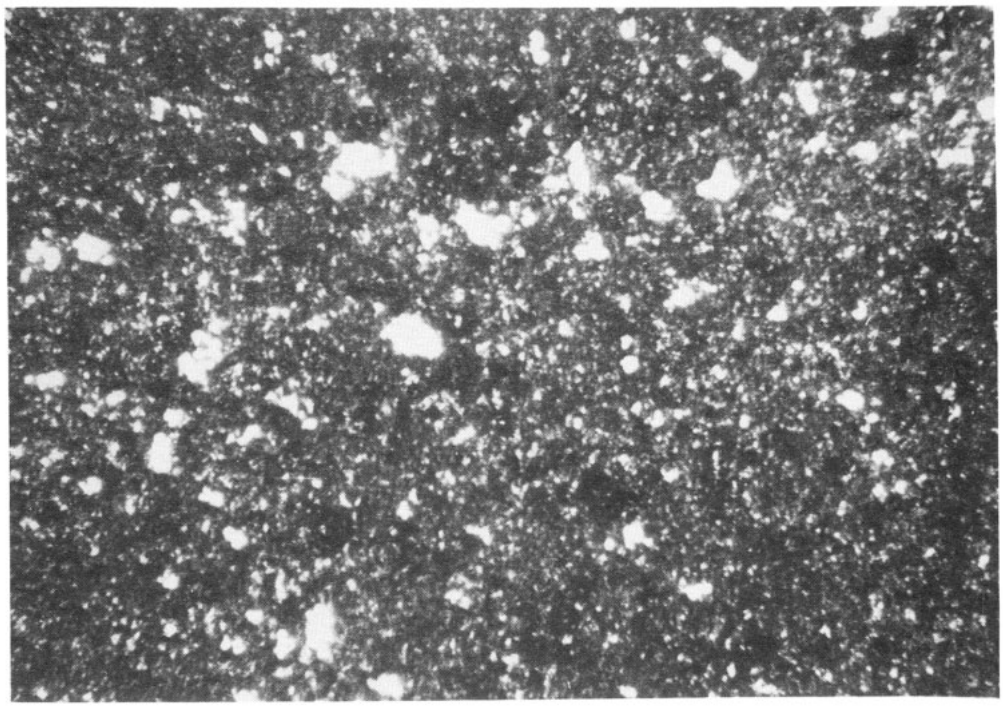

Figure 1. Optical micrograph of glass–ceramic, ×600.

exact thicknesses of the conducting layers are not known experimentally, we have calculated the surface resistivity of the specimens from the following equation:

$$R = \rho_{\square} s/w \tag{1}$$

where R is the sample resistance, $\rho_{\square}$ is the surface resistivity in ohms per square, s is the separation between the electrodes (voltage terminals) and w is the width of the specimen.

3. Results

Figure 1 is the optical micrograph of a glass–ceramic sample ceramized by heating the virgin glass at a temperature of 565 °C for 1 h followed by heat treatment at 630 °C for 3 h. The dark regions in the micrograph correspond to the glass phase whereas the light regions comprise the crystalline phase s. It is seen that the crystalline particles have sizes varying from 0.8 to 22 μm. The volume fraction of the crystalline phases is about 0.4. Figure 2 is the x-ray diffractogram of the above glass–ceramic sample. The diffraction peaks confirm the presence of the crystalline phases zinc orthosilicate (Zn_2SiO_4) and lithium phosphate ($Li_4P_2O_7$). Figure 3(*a*) is the electron micrograph of the above glass–ceramic and figure 3(*b*) is the corresponding electron diffraction pattern. In figure 3(*a*) the isolated dark features represent the crystalline phase and the light regions correspond to the glass phase. In table 1 are listed the d_{hkl}-spacings calculated from the observed diffraction rings. The standard ASTM values for the above-mentioned crystalline phases are also shown in this table for comparison. It is evident that both the crystalline phases

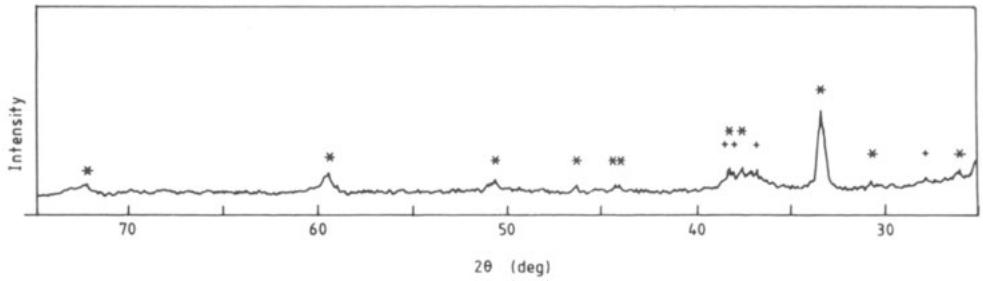

Figure 2. X-ray diffractogram of glass–ceramic: *, Zn_2SiO_4; +, $Li_4P_2O_7$.

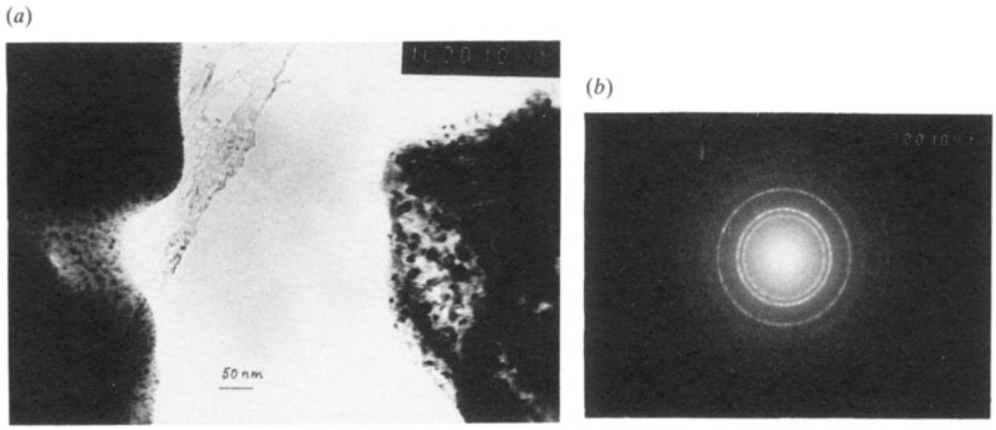

Figure 3. (*a*) Electron micrograph of glass–ceramic; (*b*) electron diffraction pattern of (*a*).

Table 1. Comparison of d_{hkl}-values from electron diffraction of the glass–ceramic of overall composition 55 mol% SiO_2–12 mol% ZnO–32.2 mol% Li_2O–0.8 mol% P_2O_5.

d_{hkl}, observed (Å)	d_{hkl}, ASTM (Å)	
	Zn_2SiO_4	$Li_4P_2O_7$
2.832	2.834	
2.417		2.410
2.145	2.144	
1.745		1.740
1.520	1.520	
1.420	1.420	

are present in the electron micrograph as well. The particle size of these phases therefore varies over a very wide range, namely from 2 nm to 22 μm.

Figure 4(*a*) is the electron micrograph of a nanocomposite consisting of a glass–ceramic in which silver particles have been grown by the reduction treatment at 340 °C for 1 h. In this micrograph the dark regions represent a silver-particle-rich phase and the light regions (e.g. A) are the orthosilicate phase. Figure 4(*b*) is the corresponding

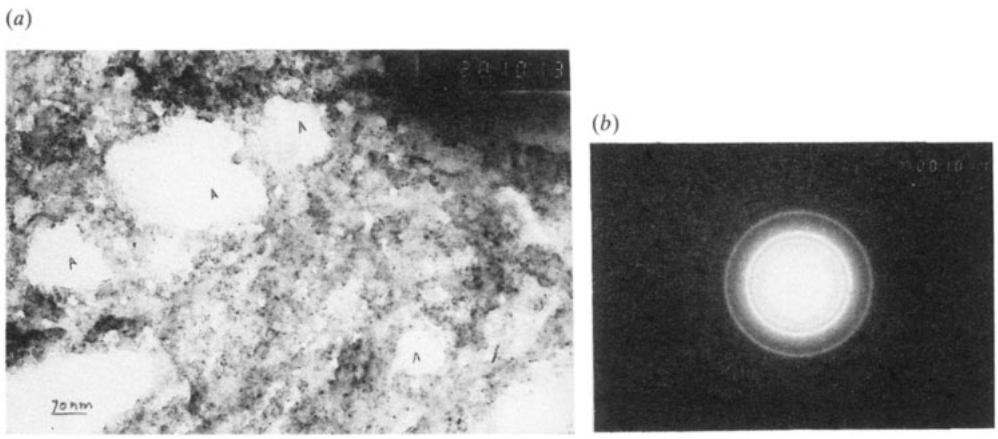

Figure 4. (*a*) Electron micrograph of nanocomposite obtained by reduction at 340 °C for 1 h. (*b*) Electron diffraction pattern of (*a*).

Table 2. Comparison of d_{hkl}-values for a silver nanocomposite involving glass–ceramic of overall composition 55 mol% SiO_2–12 mol% ZnO–32.2 mol% Li_2O–0.8 mol% P_2O_5 (reduction treatment, 340 °C for 1 h).

d_{hkl}, observed (Å)	d_{hkl}, ASTM (Å)	
	Silver	Zn_2SiO_4
2.836		2.834
2.356	2.359	
2.044	2.044	
1.441	1.445	
1.231	1.231	
1.106	1.179	
1.018	1.021	

electron diffraction pattern. Table 2 summarizes the d_{hkl}-spacings as obtained from this pattern and the standard ASTM values for metallic silver. It is evident that the ultrafine particles consist of silver. Also the presence of Zn_2SiO_4 is confirmed by one prominent diffraction ring from this phase. The micrograph indicates that the silver particles cluster around the electronically less dense Zn_2SiO_4 grains, the size of the latter as seen in this picture varying from 14 nm to 0.35 μm. The microstructure and the d_{hkl}-spacings as given for this particular sample are typical of the results obtained for all the specimens containing silver particles of different diameters. Figure 5 is a histogram of silver particles grown at a temperature of 340 °C for a duration of 1 h. We have tried to fit histograms of all samples with the log–normal distribution function

$$\Delta n = (1/\sqrt{2\pi}\ln\sigma)\exp\{-\tfrac{1}{2}[\ln(x/\bar{x})/\ln\sigma]^2\}\,\Delta(\ln x) \qquad (2)$$

where Δn is the fractional number of particles, x is the diameter, $\bar{x}$ is the median diameter and σ is the geometric standard deviation.

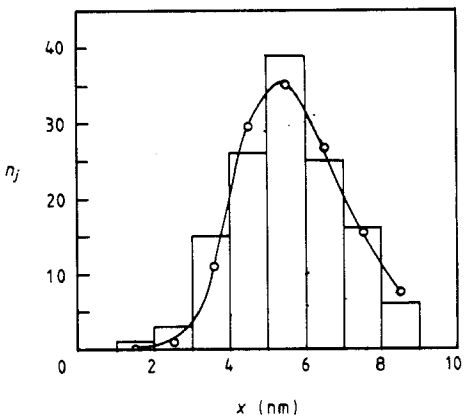

Figure 5. Histogram of silver particles grown in the glass–ceramic at the reduction temperature of 340 °C for 1 h.

Table 3. Summary of reduction treatment, silver particle diameter and standard deviation (heat treatment, 565 °C for 1 h followed by 630 °C for 3 h; ion exchange, 310 °C for 8 h).

	Log–normal distribution		Statistical averaging	
Reduction treatment	$\bar{x}$ (nm)	σ	$\bar{x}$ (nm)	σ (nm)
320 °C for 20 min	4.5	1.4	4.3	0.5
325 °C for 5 min	4.7	1.5	4.6	0.7
320 °C for 1 h	5.0	1.4	4.8	1.0
340 °C for 1 h	5.7	1.3	5.5	0.6
400 °C for 1 h	6.7	1.3	6.6	0.8
450 °C for 1 h	7.4	1.3	7.2	1.2
500 °C for 1 h	8.7	1.2	8.3	0.9
600 °C for 1 h	11.4	1.2	11.0	1.3

The full curve in figure 5 represents the curve fitted to the experimental data by equation (2). The fit does not appear to be satisfactory. We have therefore calculated the average diameter using the following relation

$$\bar{x} = \sum_{j=1}^{n} x_j \, \Delta n_j \tag{3}$$

where x_j is the diameter in the jth interval of the histogram, Δn_j the fractional number in the jth interval and n the total number of intervals. The standard deviation σ is calculated from (Chatterjee and Chakravorty 1989)

$$\sigma = \left(\sum_{j=1}^{n} (x_j - \bar{x})^2 / (N-1) \right)^{1/2} \tag{4}$$

N being the total number of particles.

In table 3 are listed the values of $\bar{x}$ and σ calculated by both the above methods for various samples subjected to different reduction treatments. The simple statistical

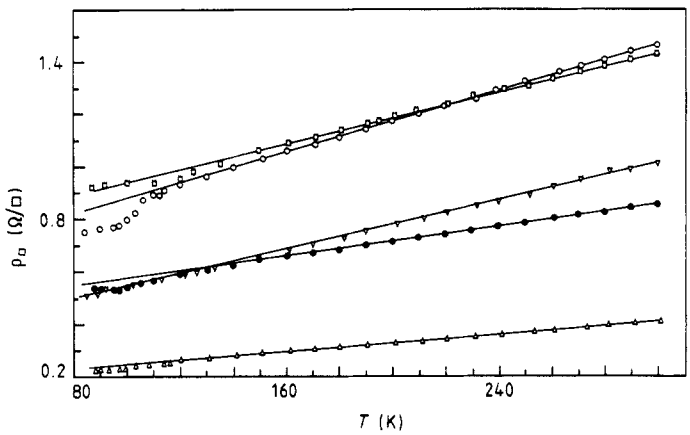

Figure 6. Surface resistivity as a function of temperature for samples with silver particle diameters ranging from 4.3 to 6.5 nm; ○, 4.3 nm; □, 4.6 nm; ▽, 4.8 nm; ●, 5.5 nm; △, 6.6 nm.

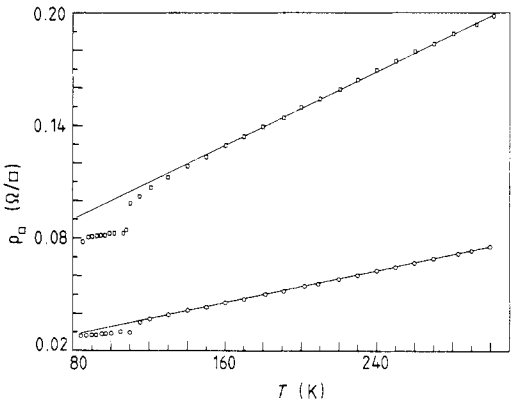

Figure 7. Surface resistivity as a function of temperature for samples with two different particle diameters: □, 8.3 nm; ○, 11.0 nm.

averaging gives a smaller value of the standard deviation than that obtained from the log–normal distribution function. The latter has been shown to be valid in the case of ultrafine particles prepared by the inert-gas evaporation technique where the growth of particles takes place by liquid-like coalescence (Granqvist and Buhrman 1976). In the present case, however, the particles are believed to be formed by a nucleation-and-growth mechanism (Das *et al* 1978). An optimum heat treatment schedule can therefore give rise to a narrow particle size distribution as reflected in the σ-values shown in the last column of table 3.

The variation in surface resistivity as a function of temperature for various samples containing silver particles of different diameters are shown in figures 6 and 7. The discrete points represent the experimental data. The full curves are the theoretical curves obtained by fitting the data to equation (5) as discussed in section 4. It is evident that the surface resistivity varies linearly over the temperature range 120–300 K. Also, the slope of this curve increases as the silver particle diameter becomes smaller. An interesting feature of the results is a break in the linear variation at a temperature of around 120 K.

Table 4. Θ_p, ρ_0 and λ for samples with different silver particle sizes.

Particle diameter (nm)	Θ_p (K)	λ (Ω K cm^{-1})	ρ_0 ($\Omega/\square$)
4.3 ± 0.5	98	110	0.61
4.6 ± 0.7	103	102	0.71
4.8 ± 1.0	105	100	0.34
5.5 ± 0.6	126	85	0.45
6.6 ± 0.8	154	75	0.18
7.2 ± 1.2	155	74	0.16
8.3 ± 0.9	163	50	0.06
11.0 ± 1.3	192	30	0.01

The slope at a lower temperature is smaller than that observed before the transition. These results are discussed in the next section.

4. Discussion

From the microstructural data presented in the previous section it is concluded that the silver particles grow preferentially at the interface of the crystalline phases and the glass matrix. The chains of these silver particles give rise to the metallic conductivity as measured in the different nanocomposites investigated here.

The effect of particle size on the electrical resistivity can be analysed in terms of the expression derived by Ziman (1960) for the lattice resistivity ρ_L of the bulk metal as follows:

$$\rho_L = C/\Theta_p(T/\Theta_p)^5 J_5(\Theta_p/T) \tag{5}$$

where Θ_p is the Debye temperature, T is the temperature, C is a constant and

$$J_5(z) = \int_0^z \frac{z^5\,\mathrm{d}z}{[\exp(z)-1][1-\exp(-z)]}. \tag{6}$$

In the present measurement system which deals with the surface resistivity the constant C is to be replaced by another constant $\lambda(\equiv C/t)$, where t is the thickness of the conducting film. We have fitted the experimental resistivities of different samples to equation (5) using λ and Θ_p as the parameters. We find that, whereas λ and Θ_p fit the slope of the experimental curve, a temperature-independent parameter ρ_0 is needed to match the experimental data. The equation used to fit the resistivity results in the present investigation can therefore be written as

$$\rho = \rho_0 + \rho_L. \tag{7}$$

Table 4 summarizes the values of λ, Θ_p and ρ_0 for silver particles of different diameters. It is evident from these results that the effective Debye temperature decreases as the particle size of silver becomes smaller. This is ascribed to the softening of the phonon spectrum due to the effect of the surface of the metal particles (Fujita *et al* 1976). It is to be noted that by the present ion-exchange technique it has been possible to grow

silver particles of diameter as small as 4.3 nm whereas the smallest size measured by Fujita *et al* (1976) was 10 nm. The lowest effective Debye temperature observed in our materials is 98 K which is substantially smaller than the value of 220 K reported for bulk silver (Ziman 1960). The decrease in the value of λ as the particle size increases is essentially due to an increase in the thickness of the conducting film. Samples with larger silver particles are prepared by subjecting the ion-exchanged sample to reduction treatment at higher temperatures for a longer duration. Such a situation enhances the diffusion of hydrogen atoms within the glass phase, thereby increasing the depth of the conducting layer formed after reduction treatment.

The temperature-independent term ρ_0 arises owing to impurity atoms or line defects within the metallic grains (Fujita *et al* 1976). It is not possible at this stage to delineate the defects present in the silver particles. The decrease in the value of ρ_0 as the particle size increases, however, can be explained on the basis of the increased thickness of the conducting layer as mentioned above.

The electron micrographs and the electrical resistivity data of the different specimens studied here indicate that there are large chain-like clusters formed by silver particles within the nanocomposites prepared. We have therefore characterized these microstructures in terms of fractal dimension (Forrest and Witten 1979). The micrograph is first digitized by hand to produce a matrix of ones and blanks corresponding to the presence or absence of a particle. Different squares are then chosen in the image and the number N of ones in each square is counted. The number N is analysed according to the power law

$$N \propto l^D \tag{8}$$

where l is the size of the square chosen and D the fractal dimension.

Figures 8(a) and 8(b) are the electron micrograph and the corresponding digitized image, respectively, of a sample containing silver particles of average diameter 11 nm. In figure 9 a plot of ln N versus ln l is shown. The data points are least squares fitted to a line whose slope gives the value of D. In table 5 the fractal dimensions obtained from the micrographs of different specimens are summarized. It is evident that the fractal dimensions of the chain-like aggregates fall roughly into two regions, namely around 1.6 and 1.9. The data presented here span only a limited range of l, i.e. 1–10. It is thus likely that the samples under investigation have clusters of two different fractal dimensions of the above magnitude. A large fractal dimension for samples with a small value of average particle diameter signifies a decrease in the surface roughness of the overall chain-like aggregate which would then behave as if it consists of large metallic particles.

The fractal structure of the silver nanoparticles has been analysed from the two-dimensional measurements on electron micrographs of the different composites. In order to assess the validity of the Hausdorff dimensions so derived in explaining the electrical resistivity behaviour of the samples concerned it is necessary to estimate the thickness of the conducting layer that we are dealing with. For this purpose we polished off successive layers of the sample surface and measured the surface resistance until we came to a stage where the latter had a value greater than $10^3\ \Omega$. The thickness of the layer removed is then taken to be a measure of the required value. We find that this thickness has a value of 20 ($\pm$5) μm for the sample with x = 4.3 nm and 55 ($\pm$5) μm for the sample with x = 11.0 nm. Thus in our measurements we are essentially dealing with the electrical properties of a three-dimensional system. However, as mentioned previously, electrical conduction occurs in the present system because of the presence

(*a*)

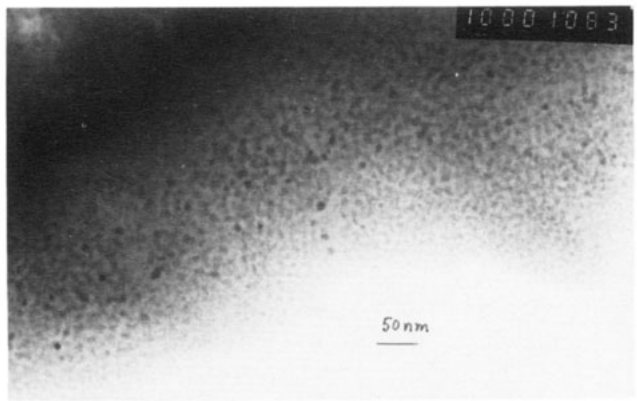

(*b*)

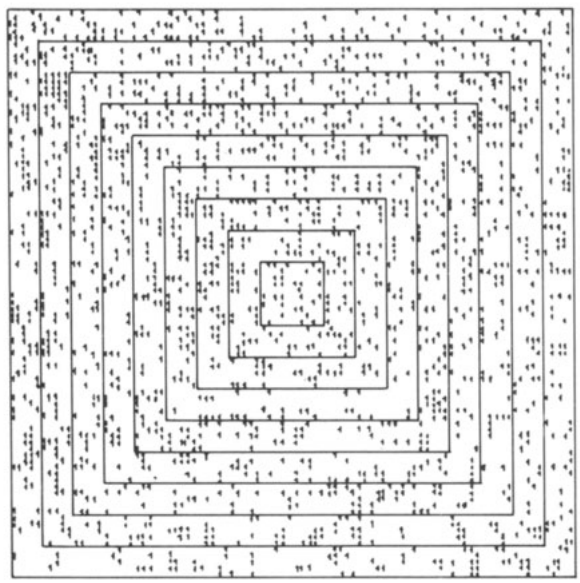

Figure 8. (*a*) Electron micrograph of glass–ceramic containing silver particles with an average diameter of 11 nm. (*b*) Digitized image of (*a*) (box size, 300 nm).

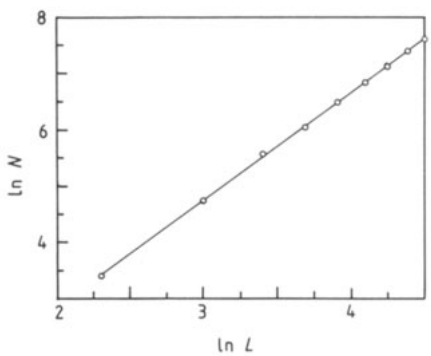

Figure 9. Ln N versus ln l plot of figure 8(*b*).

Table 5. Fractal dimensions in different samples containing silver nanoparticles.

Reduction treatment	D
320 °C for 20 min	1.65 ± 0.05
325 °C for 5 min	1.71 ± 0.08
320 °C for 1 h	1.96 ± 0.004
340 °C for 1 h	1.56 ± 0.08
400 °C for 1 h	1.94 ± 0.05
450 °C for 1 h	1.60 ± 0.2
500 °C for 1 h	1.91 ± 0.04
600 °C for 1 h	1.91 ± 0.01

of finite chain-like metal clusters formed by the nucleation and growth of these particles at the glass–crystal interface. Using the thickness values quoted above, the calculated resistivity of the conducting layer is found to be 6.0×10^{-3} Ω cm which is about 4×10^3 times higher than the bulk resistivity of metallic silver (Hodgman 1962). This provides confirmation of the presence of chain-like metal aggregates in our samples. The fractal dimensions deduced as above therefore characterize the structural features of these aggregates which occupy a three-dimensional space and control the electrical conductance of the latter.

The method of sample preparation for electron microscopy as adopted in our study precludes the delineation of morphology as a function of depth of the conducting layer. However, this method gives us a way of sampling the microstructure at various depths in a random fashion. In fact, the values of fractal dimension quoted in table 5 are an indication of the total lack of correlation between D and the preparation conditions except that they lie around two values, namely 1.6 and 1.9. It appears that the D-values depend essentially on the morphology of the glass–crystal composite precursor. As the smallest crystalline particles have a large surface-to-volume ratio, they will give rise to a larger number of metal nuclei at their surfaces than those nucleated on larger crystalline particles (Guy and Hren 1974). In the former case it is expected that the fractal dimension of the metal clusters would be higher than in the latter situation. The two values of D at around 1.9 and 1.6 reflect these conditions in our nanocomposites. It should be noted that the above line of argument should lead to the existence of a multi-fractal system in our samples. A more involved computation should be able to delineate the whole spectrum of generalized fractal dimensions (Grassberger and Procaccia 1984). However, it seems that in our nanocomposites the resistivity break as a function of temperature can be explained on the basis of the two terminal values in a spectrum of fractal dimensions.

On the basis of discussions presented above, it is evident that the metal clusters of different fractal dimensions are in a series configuration within the conducting layer of the different nanocomposites. As explained before, a cluster of larger fractal dimension would behave as if it consisted of large metal particles with a large effective Debye temperature. At around 120 K therefore such clusters dominate the temperature variation in resistivity, bringing about the observed break in the resistivity versus temperature plots. The decrease in slope of these curves below the so-called transition temperature confirms that the effective Debye temperature of the controlling cluster is higher than that exhibited by the system at higher temperatures. An extension of the

electrical conductivity measurements to temperatures below 80 K should throw further light on this problem.

Acknowledgments

The authors thank the Department of Science and Technology, Government of India, for supporting this investigation. The electron microscopy work has been carried out at RSIC, Bose Institute, Calcutta. The authors also acknowledge the help of Mr Santanu Das Gupta in some of the computational work.

References

Anderson A, Hunderi O and Granqvist C G 1980 *J. Appl. Phys.* **57** 757
Chakravorty D and Roy D 1985 *J. Mater. Sci. Lett.* **4** 1014
Chatterjee A and Chakravorty D 1989 *J. Phys. D: Appl. Phys.* **22** 1386
Das G C, Reddy T K and Chakravorty D 1978 *J. Mater. Sci.* **13** 2211
Dupree R and Smithard M A 1972 *J. Phys. C: Solid State Phys.* **5** 408
Forrest S R and Witten T A 1979 *J. Phys. A: Math. Gen.* **12** L109
Fujita T, Ohshima K and Kuroishi T 1976 *J. Phys. Soc. Japan* **40** 90
Fujita T, Ohshima K and Wada N 1969 *J. Phys. Soc. Japan* **27** 1459
Gorkov L P and Eliashberg G M 1965 *Zh. Eksp. Teor. Fiz.* **48** 1407 (Engl. Transl. 1965 *Sov. Phys.–JETP* **21** 940)
Granqvist C G and Buhrman R A 1976 *J. Appl. Phys.* **47** 2200
Grassberger P and Procaccia I 1984 *Physica* D **13** 34
Guy A G and Hren J J 1974 *Elements of Physical Metallurgy* (Reading, MA: Addison-Wesley)
Hanamura E 1988 *Phys. Rev.* B **37** 1273
Hodgman C D (ed) 1962 *Handbook of Chemistry and Physics* (Cleveland, OH: Chemical Rubber) p 2669
Marlow W H (ed) 1982 *Aerosol Microphysics* II (Berlin: Springer)
Meier F and Wyder P 1972 *Phys. Lett.* **39A** 51
Novotny V and Meincke P P 1973 *Phys. Rev.* B **8** 4168
Schmitt-Ott A, Schurtenberger P and Siegman H C 1980 *Phys. Rev. Lett.* **45** 1284
Strassler S and Rice M J 1972 *Phys. Rev.* B **6** 2575
Trotter D M and Smith D W 1984 *Appl. Phys. Lett.* **45** 112
Warnock J and Awschalom D D 1985 *Phys. Rev.* B **32** 5529
Ziman J M 1960 *Electrons and Phonons* (Oxford: Clarendon) p 364